IEEE Access
Multidisciplinary | Rapid Review | Open Access Journal

Received May 11, 2021, accepted May 28, 2021, date of publication June 7, 2021, date of current version June 21, 2021.

Digital Object Identifier 10.1109/ACCESS.2021.3086820

Underwater Optical Imaging: Key Technologies and Applications Review

YING SHEN, CHUANJIANG ZHAO, YU LIU, SHU WANG, AND FENG HUANG
College of Mechanical Engineering and Automation, Fuzhou University, Fuzhou 350116, China

Corresponding author: Yu Liu (liuyu19@fzu.edu.cn)

This work was supported by the National Natural Science Foundation of China (NSFC) under Grant 62005049.

ABSTRACT The challenges associated with acquiring the clear images of objects in underwater environment are difficult to overcome due to the absorptive and scattering nature of seawater. Recently, the research community has focused on mitigating these effects. The recent developments in image enhancement algorithms and strategies of signal light enhancement have brought improvement in some application areas. In this work, we review the six most common methods based on signal light enhancement. We present the individual working mechanisms, latest representative advances, and suitable application conditions. Moreover, we also present a detailed comparison of these techniques. In each technique, we present their applicable environments and conditions according to the following indicators: operating distance (from 2 attenuation lengths (AL) to 13.5 AL), resolution (from centimeter to millimeter), and field of view (FOV). By summarizing and analyzing the existing problems that restrict the underwater optical imaging techniques, the future development trends are prospected.

INDEX TERMS Underwater optical imaging, underwater imaging model, signal light enhancement, optical properties of seawater.

I. INTRODUCTION

The oceans occupy approximately 71% of the earth's surface of which 95% area is unexploited. In various applications, the underwater imaging technology is crucial for understanding and exploring the ocean. For instance, in military, this technology can be used for mapping the environment around the submarine and underwater minesweeping. Similarly, in scientific research, this technology is used for in-situ detection of marine life and underwater archaeology, etc. The civil use of this technology includes marine mineral exploration and underwater rescue, etc. Currently, there are two types of technical methods adopted for underwater imaging, which include acoustic imaging and optical imaging. It is noteworthy that the propagation of acoustic waves is not affected significantly by the water and dissolved impurities. Consequently, the acoustic imaging has a long detection range and covers wide area. However, the spatial resolution of acoustic imaging is poor, and it is unable to meet the requirements of high-resolution imaging. Contrary, the optical imaging has the ability to acquire intuitive and high-resolution images. However, the range of optical imaging is shorter due to high absorption and scattering of light waves caused by the seawater during propagation. Therefore, there is a need to devise some special optical imaging methods to improve the imaging range and quality of the underwater imaging systems.

The applications of underwater optical imaging include airborne sea surface detectors, shipborne underwater optical detectors, and submarine-borne optical cameras. This is presented in Fig. 1. As compared with the atmospheric imaging technologies, the underwater imaging technologies focus on reducing the impact of attenuation, such as strong absorption and scattering of light caused by water on the quality of the acquired underwater images. Especially in turbid water, the visibility is significantly less as compared to the atmosphere because the scattered background light is strong and the signal extraction is more difficult. As a result, the requirements for underwater imaging are more stringent. Based on the techniques used for suppressing the influence of underwater scattering medium, the underwater optical imaging technology is divided into two categories. The first category uses the image enhancement techniques and the second category employs signal light enhancement techniques. The intensity of the target signal light can be enhanced considerably by using different algorithms and specific hardware. In addition, the influence of the scattered

The associate editor coordinating the review of this manuscript and approving it for publication was Sukhdev Roy.

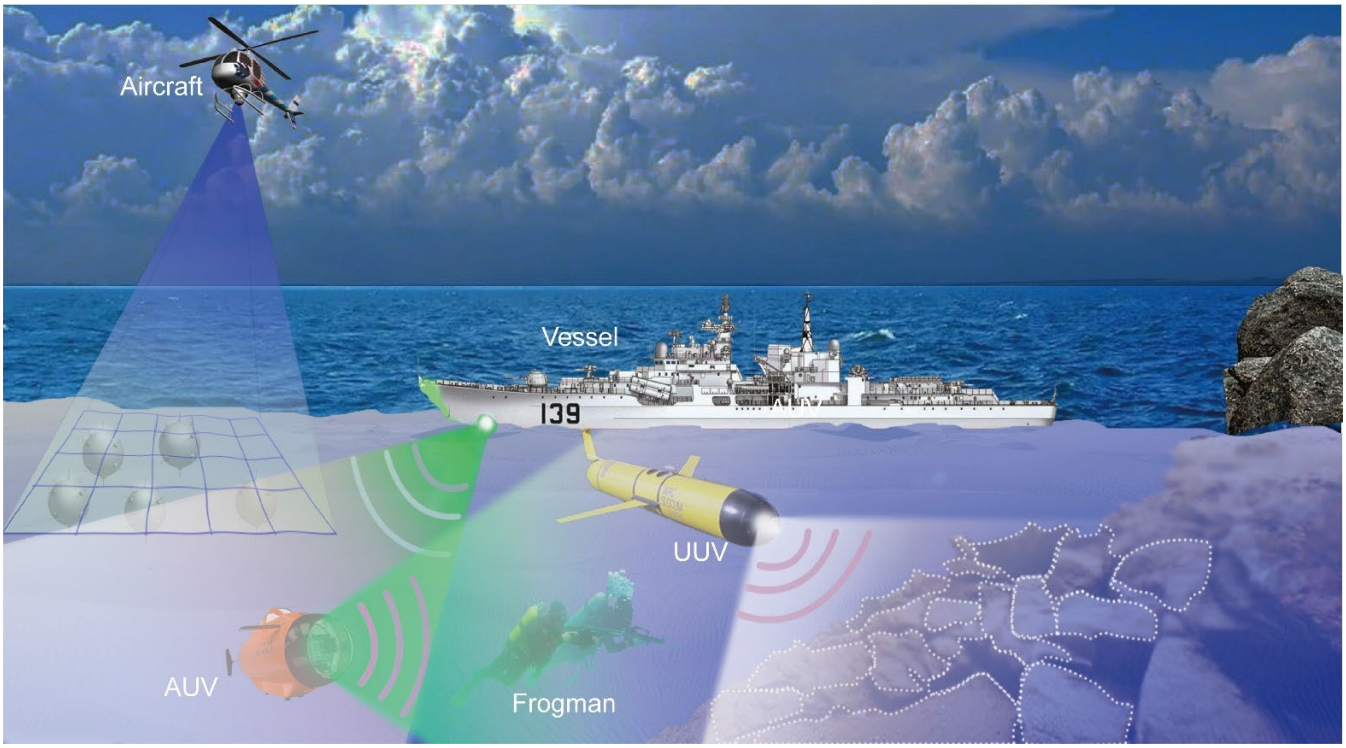

FIGURE 1. The demand of underwater target optical detection.

background light is also suppressed, which leads to contrast enhancement of the detected image.

The image enhancement methods have evolved from simple image processing techniques to image processing techniques that rely on underwater image formation models (IFM). The simple image processing methods mainly include histogram equalization (HE) [1], [2], Retinex algorithm [3]–[5], homomorphic filtering (HF) [6], wavelet transform (WT) [7], [8] and fusion [9], [10]. It is notable that these methods do not require a priori knowledge of the detected environment, which greatly reduces the computational complexity of the process. However, these methods do not consider the fundamental reasons of image degradation, due to which the processed images are unable to represent the original information accurately. In addition, the details in the output images are not enhanced enough and the output images also suffer noise amplification.

The image processing methods based on IFM include dark channel prior (DCP) [11] and its improved forms [12]–[15], and network based methods [16]–[18]. These methods mainly processed by algorithms, and the systems structure are simple, however, there still exist many problems, such as halo, chromatic aberration, and dependence of special scene which affect the output. Finally, for both of the aforementioned image enhancement techniques, the fundamental limits of hardware set the ultimate constraints on the detection range and imaging resolution.

The signal light enhancement methods are based on the scattering models or physical properties of scattering. Based on the novel imaging mechanisms, the whole imaging system is changed and improved to directly restore the underwater images. This includes range-gated imaging [19], laser synchronous scanning [20], streak tube imaging [21], polarization imaging [22], spectral imaging [23], and ghost imaging [24]. Table 1 presents the comparison between various underwater optical imaging techniques. In terms of operating distance, the range-gated imaging, laser synchronous scanning, and ghost imaging have the ability to realize long-range detection. In terms of detection field of view (FOV), the laser synchronous scanning and streak tube imaging obtain a larger FOV. In terms of imaging quality, the streak tube imaging, spectral imaging, and ghost imaging have the ability to realize a high imaging resolution.

The rest of the manuscript is organized as follows.

In Section II, we present the theoretical basis of underwater imaging. In Section III, we present the overview of underwater optical imaging based on signal light enhancement techniques. Finally, in Section IV, we summarize the developments and applications of underwater optical imaging technologies.

II. THEORETICAL FUNDAMENTAL

A. INHERENT OPTICAL PROPERTIES (IOPs) OF SEAWATER

The IOPs of seawater are the properties of the medium and are not affected by environmental factors, which are the basis for underwater optical imaging research. The main parameters are absorption coefficient, scattering coefficient, attenuation coefficient, and volume scattering function (VSF), where absorption coefficient and VSF are the two most basic parameters. In fact, beam attenuation involves two basic processes,

TABLE 1. Comparison of underwater optical imaging technologies.

	Methods	Environmental adaptation	Advantages	Disadvantages	Operating distance
Image Enhancement	HE [1, 2]	Clear Water	The algorithm is simple, Easy to hardware	Limited local information processing capability, High-frequency losses	-
	Retinex [3-5]	Clear Water	Pure algorithmic processing, The system structure is simple	Halation phenomenon, High-frequency losses	-
	DCP [11-15]	Clear Water	Pure algorithmic processing, The system structure is simple	Scene Dependence, Chromatic aberration distortion	-
	Network-based [16-18]	Clear Water	Pure algorithmic processing, The system structure is simple	Scene Dependence, Halation phenomenon, Difficulty in acquiring realistic underwater scenario datasets	-
Signal Light Enhancement	Range-gated [28-38]	Low turbidity water	Long imaging range, No mechanical scanning structure, Range accuracy measurement is not affected by distance	High cost, Small FOV, Only detect targets at a specific distance	6AL
	laser synchronous scanning [40-46]	Low turbidity water	Long imaging range, High imaging accuracy, Large FOV	Large volume, High cost, Required mechanical scanning structure	7AL
	streak tube imaging [47-52]	Low turbidity water	Large FOV, High range resolution, High detection sensitivity	Required high voltage power supply, Short service life, Poor reliability	4-5AL
	Polarization Imaging [56-62]	high turbidity water	The system structure is simple, marked contrast enhancement, High turbidity underwater imaging	Scene Dependence, Short detection distance, Large energy attenuation of the target reflected light by the polarizer	2-3AL
	spectral imaging [67-77]	Low turbidity water	High spectral resolution, High spatial resolution, Detectable spectral characteristics of the target	Complex system structure, Huge amount of data, Short detection distance	2-3AL
	Ghost imaging [80-83]	high turbidity water	High contrast imaging, High signal-to-noise ratio Long detection distance,	Complex system structure, High performance requirements of the device, Slow imaging speed	13.5AL

namely absorption, where photos are incorporated into the medium or its components, and scattering, where photons deviate from their original path into other directions. Thus, it can be expressed as a sum of these two contributions, namely

$$c(\lambda) = a(\lambda) + b(\lambda) \tag{1}$$

where λ represents the wavelength of beam, $a(\lambda)$, $b(\lambda)$, and $c(\lambda)$ represent absorption coefficient, scattering coefficient, and total attenuation coefficient, respectively.

VSF represents the scattered intensity in per unit incident irradiance with per unit volume. It is defined as the limit of this fraction as $\Delta r \to 0$ and $\Delta\Omega \to 0$:

$$\beta(\theta, \lambda) \equiv \lim_{\Delta r \to 0} \lim_{\Delta\Omega \to 0} \frac{B(\theta, \lambda)}{\Delta r \Delta\Omega} = \lim_{\Delta r \to 0} \lim_{\Delta\Omega \to 0} \frac{\phi_s(\theta, \lambda)}{\phi_i \Delta r \Delta\Omega} \tag{2}$$

where $B(\theta, \lambda)$ represents the scattered energy within the scattering angle of θ and solid angle $\Delta\Omega$, Δr is the thickness of water, $\phi_s(\theta, \lambda)$ and ϕ_i represent the energy of all scattered beams and the incident beam, respectively. The scattering coefficient can be obtained through integrating the VSF in the full solid angle.

$$b(\lambda) = \int \beta(\theta, \lambda) d\Omega = 2\pi \int_0^{\pi} \beta(\theta, \lambda) \sin\theta d\theta \tag{3}$$

The scattering is azimuthally symmetric about the incident direction, which is divided into two parts: forward scattering b_f and backscattering b_b, respectively.

$$\begin{aligned} b_f(\lambda) &= 2\pi \int_0^{\pi/2} \beta(\theta, \lambda) \sin\theta d\theta \\ b_b(\lambda) &= 2\pi \int_{\pi/2}^{\pi} \beta(\theta, \lambda) \sin\theta d\theta \end{aligned} \tag{4}$$

In underwater optical imaging, forward scattered light causes images degraded in resolution, whereas backward scattered light causes images degraded in contrast.

When a monochromatic collimated beam propagates in water, the intensity of output light decreases exponentially

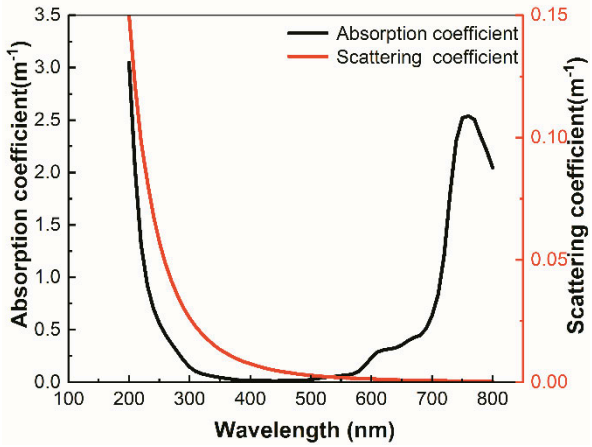

FIGURE 2. Absorption coefficient and scattering coefficient in seawater [25].

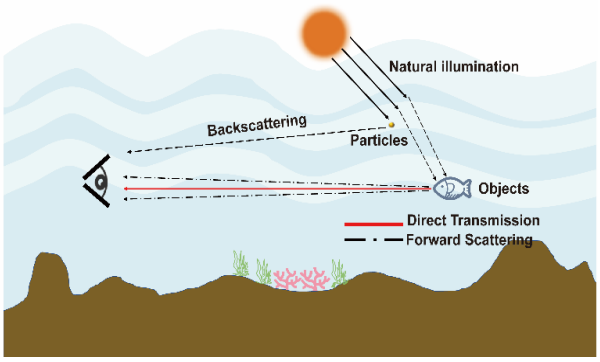

FIGURE 3. Absorption coefficient and scattering coefficient in seawater.

with water depth, following the exponential decay law (Beer-Lambert law).

$$I(\lambda) = I_0(\lambda)\, e^{-c(\lambda)L} \tag{5}$$

where L represents the transmission distance of light in water, $I_0(\lambda)$ and $I(\lambda)$ represent the input and output light intensity, respectively.

In 1981, Smith and Baker [25] measured the absorption and scattering coefficients of seawater in 200-800 nm, the result is presented in Fig. 2. The spectral absorption coefficients of seawater are higher in both the infrared (IR) and ultraviolet (UV) bands, because water molecules resonate strongly with the light in the UV and IR bands (UV absorption corresponds to a transition of bonded electron to excited-state lone pair electron, IR absorption corresponds to a transition between water molecule vibrational energy levels), while in the visible (VIS) band, this resonance is relatively weaker, so the absorption of light is weaker as well. For pure seawater, scattering is dominated by Rayleigh scattering, whose scattering intensity is inversely proportional to the fourth power of the wavelength, hence the scattering coefficient decreases with increasing wavelength. In the blue-green spectral region with a wavelength of 450-570 nm, the absorption and scattering coefficients of seawater are both small, thus becoming the optimal transmission window of light in oceanic environments. This is one of the primary reasons for that the 532-nm laser is the most widely used light source in underwater optical applications.

B. UNDERWATER IMAGING FORMATION MODEL (IFM)

The IFM is the basis of underwater image recovery. The diagram of light beam propagation in water is presented in Fig. 3, the light information received by the detector mainly consists of three parts [26]: a) The light reflected from the target after absorption and scattering by the medium (direct transmission); b) the light reflected from the target is scattered by the suspended particles at a small angle(forward scattering); and c) the light reflected by suspended particles without passing through the target object(backscattering). Since the effect on the image caused by forward scattering is very little, thus it is generally ignored when considering image degradation, then the IFM can be represented as follows:

$$\begin{aligned} I(x,y) &= D(x,y) + B(x,y) \\ &= \mathrm{J}(x,y) \cdot t(x,y) + A_\infty (1 - t(x,y)) \end{aligned} \tag{6}$$

where $D(x,y)$ represents the direct transmission and $B(x,y)$ represents the backscatter. $I(x,y)$, $J(x,y)$, and A_∞ is the captured images, images without scattering, and the homogenous background light, respectively. $t(x,y)$ is the transmissivity, which describes the attenuation of light during propagation, usually related to the depth of the field (DOP) and attenuation coefficient. It can be presented as:

$$t(x,y) = e^{-c(\lambda)d(x,y)} \tag{7}$$

where $d(x,y)$ represents the DOP, that is, the distance between the target and the camera.

According to (6) and (7), the transmissivity $t(x,y)$ and the image without scattering $J(x,y)$ can be calculated:

$$t(x,y) = 1 - \frac{B(x,y)}{A_\infty} \tag{8}$$

$$J(x,y) = \frac{I(x,y) - A_\infty [1 - t(x,y)]}{t(x,y)} \tag{9}$$

From (8), it can be seen that the transmissivity is related to the background scattering. From (9), it can be seen that as long as the water transmissivity and the homogenous background light are estimated, the underwater image without scattering can be inferred.

The methods such as range-gated imaging [19], laser synchronous scanning [20], and streak tube imaging [21] have eliminated stray light through temporal or spatial separation, the obtained images are the mixture of medium transmittance and target image. Polarization imaging [22] and ghost imaging [24] both consider the medium transmittance, and the obtained images are closest to the initial target image.

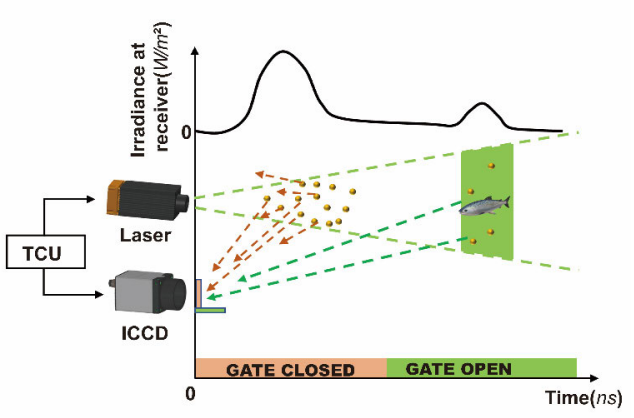

FIGURE 4. The principle of underwater laser range-gated imaging.

III. UNDERWATER IMAGING BASED ON SIGNAL LIGHT ENHANCEMENT TECHNIQUES

A. RANGE-GATED IMAGING

Range-gated technique was proposed by Heckman [27] in the 1960s, due to its effectiveness in eliminating the effect of backscattered light and in obtaining depth information of the target, it has become the main means to achieve long-range detection in harsh environments such as fog, dust, and underwater.

The range-gated imaging system is primarily composed of a high-power pulse laser, a timing control unit (TCU), and an intensified CCD (ICCD). Its imaging mechanism is presented in Fig. 4. This method is based on the principle of time of flight (TOF) with precise time delay control and ICCD ultrafast gated, which allows the camera to only receive laser pulses reflected from the target area, separating most of the background scattered light from the target signal light and improving the imaging resolution. Besides, high energy of the pulse laser offsets the signal consumption caused by water, which increases the working distance of the system. Moreover, it acquires a set of 2D slice images at different distances by time-delayed stepping scanning, and can realize 3D imaging by using the ''time-space'' mapping relationship of these slice images. The range resolution of the system is determined by the laser pulse width and camera gate width. The narrower they are, the higher signal-to-noise ratio (SNR) of the imaging.

Range-gated imaging can achieve underwater 3D imaging. According to the difference of 3D reconstruction methods, they can be classified into time-slicing 3D imaging [28] and range-intensity correlation (RIC) 3D imaging [29], [30]. The time-slicing 3D imaging technique uses high-precision time-delayed stepping scanning to acquire multiple gated slice images for 3D reconstruction. However, it still exists the problems of mass data and poor real-time performance. The RIC method uses two spatially overlapping gated images to reconstruct 3D spatial information by the mapping relationship between the intensity and range, which overcomes the rigorous demand of the mass data of time-slice 3D imaging

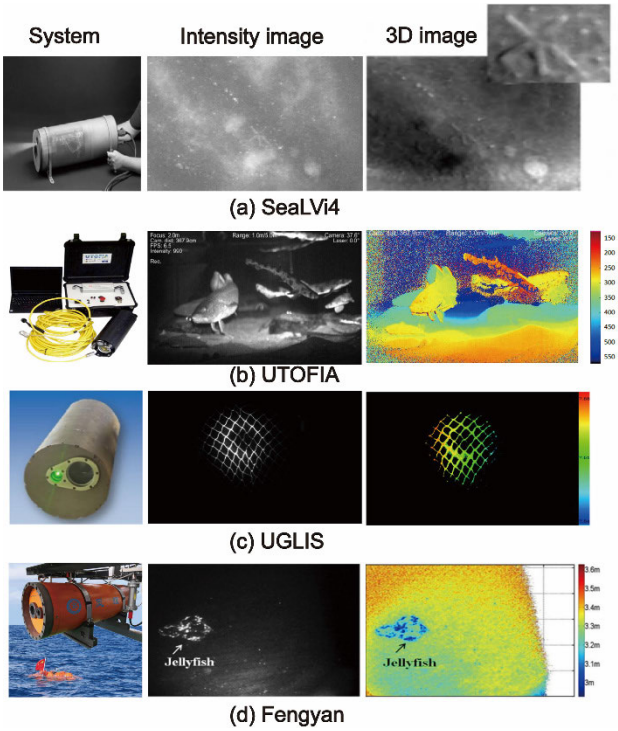

FIGURE 5. Four range-gated imaging systems and their images [31], [32].

and realizes real-time 3D imaging. According to the different range intensity envelope characteristics of the gated image, it can be divided into trapezoidal RIC 3D imaging [30] and triangular RIC 3D imaging [29]. The range resolution of the latter is four times higher than that of the former, and is superior in high range resolution of 3D imaging.

There are two main strategies for underwater range-gated imaging. One is underwater fast-moving target imaging, this kind of system has a short exposure time and high-resolution imaging. However, the size and power consumption of this system are large, which is only suitable for underwater platforms like autonomous underwater vehicle (AUV) and unmanned underwater vehicle (UUV). Another one is underwater portable application, both the size and the power consumption of which are small. It is suitably to be equipped in a frogman to work for underwater rescue and archaeology.

Typical underwater range-gated imaging systems and their imaging results in recent years are shown in Fig. 5 [31], [32]. In 2014, Christnacher *et al.* [32] developed SeaLVi4 system, which employs a 21 kHz repetition frequency and 2 ns pulse width laser at 532 nm with 170 mW of power to illuminate a FOV of 17° × 13°. The system was tested in Baltic Sea [33] with an attenuation coefficient of 0.5 m^{-1}. The result is presented in Fig. 5(a), it realized the 3D reconstruction of starfishes with a range resolution of centimeter. In 2015, seven European countries including Denmark, Spain, Norway, Germany, Italy, France, and the UK spent €5.7 million on the development of underwater time of flight image acquisition (UTOFIA) project [34], which is part

of the EU's Horizon 2020 program and commercialization in 2018. This system is mainly used for marine biomonitoring, marine litter detection, fisheries stock assessment, and seafloor mapping. In 2018, Mariani *et al.* [19] displayed the detailed parameters of the UTOFIA system: The pulse duration, repetition frequency, and working distance are respectively 1.8 ns, 1 kHz and 4 attenuation lengths (AL). The FOV, resolution, and depth range are respectively 70° (diagonal), 1280 × 1024, and 300 m. In addition, this system can achieve real-time 3D(10Hz) imaging with a range resolution up to centimeter (as shown in Fig 5. (b)). Compared with other range-gated imaging systems, UTOFIA employs a Complementary Metal-Oxide-Semiconductor (CMOS) sensor instead of ICCD, leading to a reduction in system cost and structural complexity [35]. In 2017, Liu *et al.* [36] developed an underwater gated laser imaging system (UGLIS), which employs a 30-50 kHz repetition frequency and 8 ns pulse duration laser at 532 nm with power of 3 W to illuminate a FOV of 1-6°. For ICCD, the resolution is 1360 × 1024 and the minimum range gate is 5 ns. The imaging results are presented in Fig 5. (c), it is mainly used for long-distance detection of tiny underwater targets such as mm-level fishing nets, the detection distance reaches 5.7 AL, and the recognition accuracy reaches 93.79%. In 2018, Wang *et al.* [37] developed an underwater in-situ 3D imaging system Fengyan. It equipped a 30 kHz repetition frequency and 1ns pulse duration laser at 532 nm with power of 0.5 W. As for ICCD, the resolution is the same as UGLIS and the minimum range gate is 3 ns. The imaging results of Fengyan system are presented in Fig. 5(d), it captured a 3D video image of a jellyfish with the size of ∼5 cm and speed of ∼1.5 cm/s at 1070 m underwater in the South China Sea. The range resolution of the 3D imaging reached a level of centimeter with megapixels under a deep-sea and all-black condition. This system shown promising applications in in-situ detection and quantitative analysis of marine organisms.

Although range-gated imaging can improve the detection distance and image quality by suppressing backscattering. However, partial backscatter noise still exists in the gated image, which causes the reduction of range resolution and accuracy in 3D reconstruction. To mitigate the noise impact, Wang *et al.* [38] proposed a 3D deblurring-gated range-intensity correlation imaging (De-GRICI) method. This method is based on light propagation properties in water, and only the attenuation coefficient and a frame of the reference image are required to calculate the gated image with less noise. The results shown that De-GRICI can improve the peak signal-to-noise ratio (PSNR) of the gated image by 9 dB, which effectively improved the range resolution of 3D imaging.

Range-gated imaging technique is insensitive to the ambient light and the movement of platform. Besides, it has the advantages of long detection distance, an effective suppression of backscattering noise, and the ability to 3D imaging, which has great potential for application both in military and civilian fields. However, there still exist some fundamental restrictions to be overcome for range-gated imaging: (i) the reflectivity between different parts of a same target, and the reflectivity between the target and the environment are usually inconsistent, which lead to a distinctly different brightness in the related areas for the gated images, resulting in data voids in the 3D image and worsening its visual performance. (ii) the echo signal of the target with limited detection distance is low, and the SNR of the 2D image is small, which leads to data voids in the 3D image. With the maturity of high-power miniaturized pulsed lasers and the growing development of high-sensitivity detectors, underwater range-gated imaging technique will make progresses in the following directions: miniaturization and low power consumption; combination with other underwater imaging technologies, such as digital image processing technologies, to achieve clearer imaging of underwater long-distance targets.

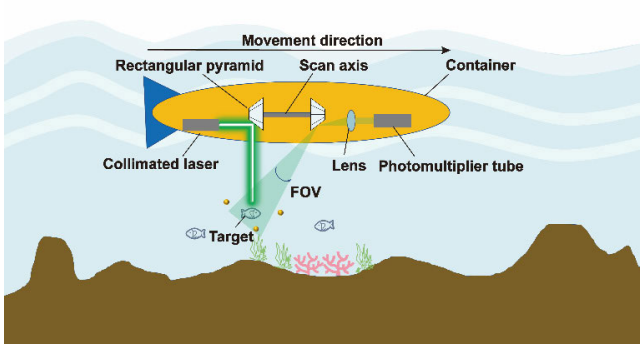

FIGURE 6. The principle of underwater laser synchronous scanning system.

B. LASER SYNCHRONOUS SCANNING

Laser synchronous scanning technique was first proposed by Rioux [39] in the 1980s, and then Jaffe and Dunn [40] applied it to underwater imaging, due to its high angular resolution and large lateral scanning FOV, it has widely been used in the fields of underwater ranging and underwater 3D reconstruction.

A typical laser synchronous scanning system is presented in Fig. 6, it includes a narrow instantaneous FOV receiver and a highly collimated laser source. Both of them are separately by adequate distance so that the area between illumined region and detected region is minimized. Hence, the backscattered light received by the detector is reduced substantially with separating the target signal light from the backscattered light spatially, which improves the imaging SNR. The depth of field of the system can be extended by using synchronous scanning, which can be achieved by mechanical synchronization and signal synchronization.

According to the difference of the sampling methods, laser synchronous scanning can be classified into three types: laser point scanning (LPS) [41], laser line scanning (LLS) [42], and laser field scanning (LFS) [20]. LPS adopts a

point-by-point scanning method with the advantages of a concentrated beam energy and high imaging resolution, however, the imaging speed is slow, which limits the practical application. Compared with LPS, LLS improves the imaging speed, and compared with range-gated imaging, LLS reduces the requirement of laser power, which makes it the most widely used method. By using Micro-Electro-Mechanical System (MEMS) micromirrors, LFS extends the laser beam into a raster pattern. Through measuring the entire surface simultaneously by phase variation, LFS leads to a fast imaging and is suitable for underwater imaging for moving target.

According to the difference of light source, LLS is classified into three categories: continuous wave LLS (CW-LLS), pulse gated LLS (PG-LLS), and modulated LLS (Mod-LLS) [43]. Similar to the ranged-gate imaging system, PG-LLS also acquires depth based on TOF. In 2009, Dalgleish *et al*. [44] compared the performance of PG-LLS and CW-LLS. The experimental results demonstrated that PG-LLS significantly improves the contrast and SNR of the image. PG-LLS was limited by forwarding backscatter at 7 AL, while CW-LLS at 6 AL. Mod-LLS employs frequency modulation in the laser source to mitigate the backscatter. In 2014, O'Connor *et al*. [45] developed a pulsed laser imaging system, which employed Radio Frequency (RF) intensity modulation on a short pulse to suppress backscatter. The results showed the contrast of output images are greatly improved. In addition, both range precision and range blurring are improved.

In conventional laser synchronous scan imaging, the imaging system needs to move vertically to extend the longitudinal FOV, meanwhile, high motion stability is required. Therefore, the laser synchronous scan system is complex and difficult to implement, despite its principle is simple. The latest research on laser synchronous scanning was focused on the improvements of system stability. In 2017, He *et al*. [46] employed five laser sources and a CMOS camera to simulate the imaging process of LLS. By employing features of the CMOS camera, such as region of interest (ROI) and rolling shutter, the system uniformly divided the image into five sub-regions along the rows. These sub-regions were scanned via changing the ROI area under the simultaneous irradiation by the sequentially triggered lasers. Compared with conventional LLS, this method reduces the mechanical complexity and improves system stability without the translation requirement of the receiver. In 2020, Wu *et al.* [20] introduced an underwater LFS system. The system equips a scientific CMOS (sCMOS) camera with short exposure time and high sensitivity to acquire a narrow FOV in rolling shutter mode. Meanwhile, a MEMS-based 2D laser scanning light source merely illuminates the narrow FOV of the camera. Therefore, it remarkably reduces the backscatter caused by the overlapped FOV of the light source and the camera without the translation requirement of the receiver. The experimental result is presented in Fig. 7, it demonstrates that LFS notably improved the contrast by 8.77 times and the contrast

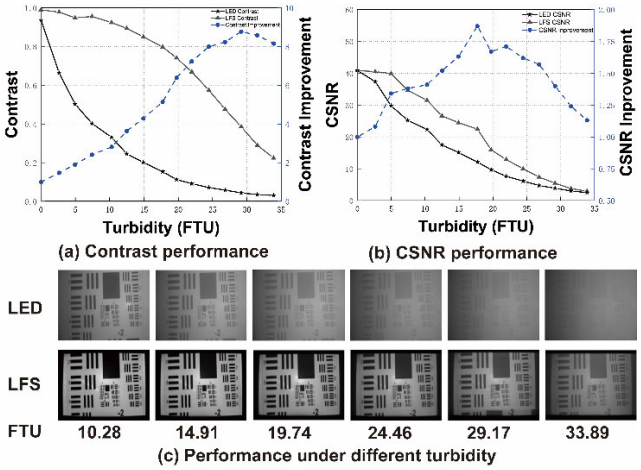

FIGURE 7. LFS system and its imaging performance [20].

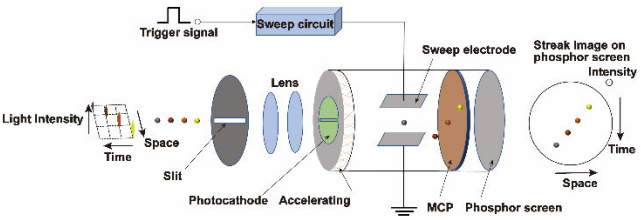

FIGURE 8. Streak tube imaging principle.

signal-to-noise ratio (CSNR) by 1.87 times compared with the LED light source.

Laser synchronous scanning technique separates signal light from backscattered light by spatial separation, which has the advantages of large FOV, long-range detection, and high resolution. In the future, the laser synchronous scanning technique will make progresses in the following directions: miniaturization, low power consumption, and high motion stability; combination with image denoising and de-fogging algorithms to achieve clearer underwater imaging at long distances.

C. STREAK TUBE IMAGING

Streak tube imaging lidar (STIL) is a novel flash imaging lidar, which was first proposed by Knight *et al.* [47] in 1989. Due to the advantages of high frame frequency, large FOV, and high resolution [48], [49], STIL has been widely used in the field of marine search and rescue, seafloor terrain detection, and torpedo detection in recent years.

As the core component of STIL, stripe tube mainly composed of photoelectric cathode, electron acceleration system, focus deflection system, microchannel plate (MCP), and phosphor screen, which are used to implement the photoelectric conversion, focus imaging, deflection scanning, and image enhancement respectively. The principle of the system is presented in Fig. 8. Firstly, the incident light signal is focused on the photocathode via the silt and lens. Then, photoelectrons reaching the deflection system at various

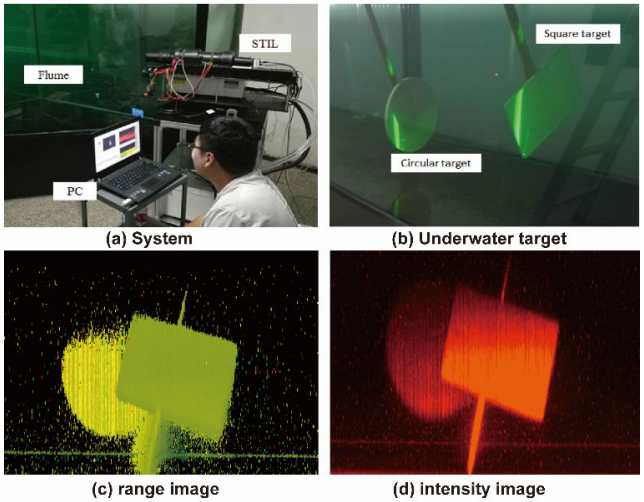

FIGURE 9. STIL system and its imaging results [21].

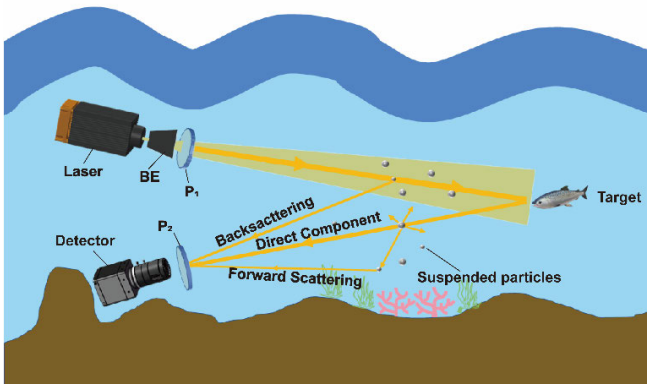

FIGURE 10. Schematic diagram of active underwater polarization imaging.

moments are separated perpendicularly to the slit under the effect of the ramp voltage. Finally, the photoelectron beam forms a striped image on the phosphor screen after being enhanced by MCP. Through imaging analysis and processing, 2D data of the incident light signal can be acquired. One dimension of the 2D data is the light intensity with spatial variation along the slit direction, another is the light intensity with time variation perpendicular to the slit direction. A series of 2D images in the direction of motion can be obtained by external mechanism push-broom, and 3D images can be acquired through 3D reconstruction based on the above time serial images.

In 2011, Gao *et al*. [50] built a STIL system, which uses a 532 nm pulse laser with pulse width of 8 ns, a repetition frequency of 100 Hz, and a pulse power of 20 mJ. The range resolution of the underwater target was 10 cm. In 2014, Tian *et al*. [51] developed a control software and constructed an image processing system for STIL using VB and MATLAB, the range resolution is better than 2 cm. In 2015, Gao *et al*. [52] carried out a series of imaging experiments using a STIL with a range resolution of 1.5 cm for underwater targets at a distance of 3 m. In 2018, Cui *et al*. [21] developed a STIL for real-time 3D imaging of underwater targets, which used a 532 nm pulse laser as the light source, the repetition frequency was 120 Hz, and the pulse duration was 8 ns. Its maximum detection depth reached 31 m with an imaging frame rate of 100 Hz. The experiment was carried out in a flume with an attenuation coefficient of 0.2 m^{-1}, the system and imaging results are presented in Fig. 9. It could acquire a real-time 3D image of a target from 22 m, whose range resolution and spatial resolution were 1 cm and 0.3 cm respectively.

The detection distance of STIL is about 4-5 attenuation lengths. Compared with the range-gated imaging, the laser energy of STIL is more concentrated, thus the depth of detection is larger [53]; compared with the single-point scanning system, the imaging system of STIL is more efficient and stable [54]. However, the STIL system still exists the following problems: (i) it requires multiple photoelectric conversion processes, resulting in huge loss of energy; (ii) the structure of streak tube is complex and it requires a driving voltage of nearly 1 kV, leading to high power consumption. With the miniaturization of the streak tube, the STIL system will develop in the following directions: miniaturized, integrated, and intellectualized.

D. POLARIZATION IMAGING

Polarization imaging was proposed by Schechner in 2003 [55], which was applied to atmospheric dehazing initially, and then the technique was promoted in the field of underwater imaging [56]. Underwater polarization imaging has the advantages of simple structure, high imaging performance, and high cost-effectiveness, which is widely used in marine resource exploitation, underwater archaeology, and underwater target identification.

Different from traditional underwater imaging, a polarized imaging system sends a beam of polarized light for the illumination and then receives echo signal with polarized information, as shown in Fig. 10. Generally speaking, underwater targets have rough surfaces, thus they have obvious depolarization effects. When a beam of polarized light illuminates the underwater scene, the signal light from target is unpolarized, while the backscattered light is partially polarized. A polarization imaging system can separate the signal light from the stray light and then reconstruct clear underwater images by using their differences in polarization properties. There are two categories for underwater polarization imaging technologies: one is the underwater image restoration methods based on polarization-difference (PD); the other one is the IFM-based polarization image restoration methods.

PD-based methods filter out background scattering noise according to the difference in the direction of light vector vibration between the target light and the background light. As shown in Fig. 11, B represents a beam of backscattered light with a polarization angle of α, and T represents the target signal light with a polarization angle of β. According

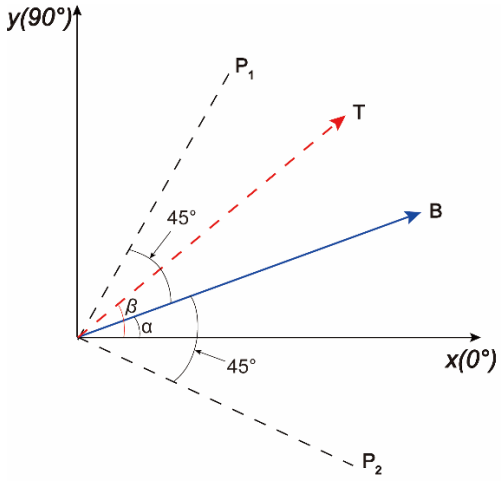

FIGURE 11. The principle of polarization difference imaging.

to Marius' law, the backscattered light can be filtered out by the common mode suppression of the polarization analyzer. And the mechanism of polarization-difference imaging is expressed as

$$I_{\mathrm{pd}}(x, y) = I_{\parallel}(x, y) - I_{\perp}(x, y) \tag{10}$$

where $I_{\parallel}(x, y)$ and $I_{\perp}(x, y)$ represent the intensity distributions obtained at two orthogonal linear polarizations.

In practical underwater detection, the polarization states of the backscattered light and target signal light are uncertain due to the complexity of the water environment, which limits the application of above methods. In 2009, Treibitz and Schechner [57] proposed a physical model for the estimation of backscattered light and target signal light. The method is implemented based on the accurate acquisition of the brightest polarized image and the darkest polarized image, which correspond to the strongest case and the weakest case of the backscattered light intensity, respectively. Methods to obtain the brightest and darkest images include subjective judgment, filter scanning [56], stokes vector estimation [58], and optical correlation evaluation [59]. Through this model, the effect of backscattered light can be removed, and then the image of object scene can be recovered.

IFM-based polarization imaging was first proposed by Schechner [60] in 2005. It estimates the seawater transmissivity by measuring the polarization of the backscattered light, and then inverts the image degradation process based on IFM. Consequently, it can realize the separation of signal light and stray light and improve the quality of underwater imaging. Compared with PD-based imaging, this method is more beneficial in obtaining the detailed information about the images and improving the image contrast. However, the traditional IFM-based polarization imaging can only recover the images of objects with low degree of polarization (DOP) (such as stones, plastics, wooden products, etc.), since the reflected light from objects with high DOP (such as metals and other smooth objects) still keeps polarized or partially polarized leading to significant errors. Considering the polarization properties of targets, Huang *et al*. [61] proposed a method based on curve fitting to estimate the orthogonal PD signal of the targets, which leads to the correct deduction of the transmittance in the scattering environment, overcoming the restriction of imaging for objects with high degree of polarization.

Numerous researches have shown that the light source properties have an impact on the quality of underwater polarization imaging. In 2014, Laan *et al*. [62] demonstrated that circularly polarized light is better able to maintain its polarization property than linear polarized light in turbid environments. Based on this research, Hu *et al*. [63] proposed an underwater polarization imaging based on an illumination of circularly polarized light in 2018, which combines circular polarization information and linear polarization information to recover image, overcoming the attenuation of polarization information and improving the quality of polarization image. The light sources employed for underwater imaging are mostly point sources, which result in a non-uniform light field in water, leading to an inhomogeneous distribution of polarization parameters. To solve this problem, Hu *et al*. [64] proposed a method of polarization image recovery under a non-uniform light field in the same year, which considers the DOP and intensity of the backscatter as spatial variables and derives their distribution functions in space through 3D fitting. It overcomes the problem that the DOP and intensity of backscattered light are in homogeneously distributed in space under a non-uniform light field, which improves the quality of the underwater image. However, when employing linear polarized light to illuminate underwater scenes, the difference in polarization states between the reflected light from target and the stray light cannot be hold any more, which causes the failure of the polarization recovery. In 2019, Yang *et al*. [65] utilized unpolarized light to illuminate the underwater scenes, which verified the polarization effect of the signal light could be ignored regardless of the DOP of the object. This special property expands the application range of underwater polarization imaging.

Image recovery in environment of highly turbid water is one of the research hotspots and also a difficulty in underwater imaging. In 2018, Liu *et al*. [22] proposed an underwater active polarization imaging method based on wavelength optimization. This method was realized based on the fact that the light scattering reduces with increasing wavelength in turbid water. It used a high-power red laser as the illumination source to minimize the scattering during propagation, and decoded the polarization information of the target scene through optical correlation principle, which alleviated the image degradation due to the strong scattering of turbid water, and then the polarized images of targets in highly turbid water were recovered. This is presented in Fig. 12.

Polarization imaging has the advantages of simple structure, low cost, and marked contrast enhancement, whose detection distance is 2-3 AL, making it suitable for underwater close-range target imaging. Besides, combined with

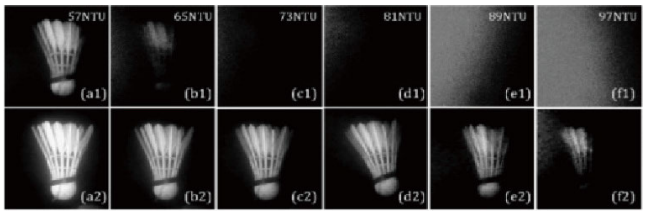

FIGURE 12. Intensity images and recovered images by wavelength optimization polarization imaging techniques in water with gradually varied turbidity [22].

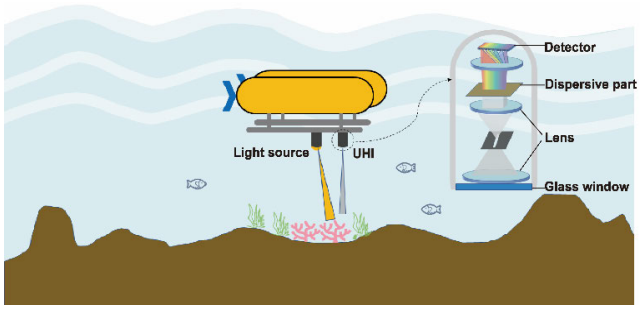

FIGURE 13. A schematic diagram of UHI system.

wavelength selection, this technique enables high turbidity underwater imaging, which has broad application prospects around the offshore areas. In the future, underwater polarization imaging will develop in the following directions: (i) improve the quality of polarization images and extract valuable polarized information from them; (ii) make use of polarized information to realize underwater polarization 3D imaging; (iii) research the changes of polarized light properties in natural water, and reduce its scene dependence and expanding its application scope.

E. SPECTRAL IMAGING

Spectral imaging is a combination of spectral technique and imaging technique, which scans each image pixel with tens to hundreds of narrow wavebands, and can obtain two-dimensional spatial information and one-dimensional spectral information of the target. This technique combines the spatial structures and spectral characteristics of the targets simultaneously, which realizes the synchronous detection of spatial dimension and spectral dimension, and provides the possibility of classification and identification of the target. Currently, spectral imaging systems based on shipborne, airborne, and spaceborne platforms have been capable of detecting objects dozens of meters underwater [66]. However, the above spectral imaging systems cannot achieve the perception of deep-sea targets due to the strong attenuation caused by water. In order to build a stereoscopic marine spectral remote sensing system with multi-scale and full depth, underwater spectral imaging was proposed.

Underwater hyperspectral imaging (UHI) system consists of three main components: hyperspectral imager, light source, and sensors, as shown in Figure 13. The underwater hyperspectral imager is the core component, which is used to acquire narrow-band spectral images of underwater targets in specific wavelength bands; the light source is used to provide illumination for underwater targets; sensors are used to correct the attenuation of light energy by the water. Due to the attenuation effect caused by water, the spectral intensity of the underwater target is different at different distances. Generally, a standard whiteboard with known reflectance is placed near the detection targets, and the reflectivity of the targets are obtained by comparing the normalized grayscale value for each pixel within the hyperspectral images.

According to the difference of imaging types, underwater spectral imaging systems can be classified into three categories: the push-broom system, the staring system, and the snapshot system. Among them, the push-broom underwater spectral imaging system acquires all the spectral data in one imaging row through prism or grating, which has the advantages of high spectral resolution and high imaging speed. However, it need to be loaded on a mobile platform to complete the image stitching, thus its imaging stability is poor, mainly used for marine mineral exploration, seafloor mapping, etc. The staring underwater spectral imaging system makes use of the selective transmission of the filter system. Therefore, only one frame of 2D image with an individual waveband is acquired by the image sensor each time, and it requires to switch the transmission band of the filter system to realize the perception of different spectral bands. The core of the system is the filter system, which includes filter wheels, a linear variable filter (LVF), an acousto-optic tunable filter (AOTF), and a liquid crystal tunable filter (LCTF). The staring underwater spectral imaging system shows a low spectral resolution and a low imaging speed, which is only appropriate for the imaging of underwater stationary targets. The snapshot underwater spectral imaging system can capture and reconstruct the spectral image data cube by single-exposure, which is suitable for the imaging of underwater moving targets with the advantage of high imaging speed, and it is the trend of underwater spectral imaging in the future.

Underwater spectral imaging is mainly concentrated in the visible band from 390 nm to 780 nm, which is caused by the strong absorption of light in the infrared band and ultraviolet bands by water. In 2013, Johnsen *et al.* [67] developed a push-broom underwater hyperspectral imagery (UHI) system based on grating diffraction. The detection band range, the number of bands, the spectral resolution, and the detection range of the UHI system are respectively 400-720 nm, 150-200, 2.2-5.5 nm, and 0.2-5 m. This system was the only one commercial underwater spectral imaging system, which was mainly used for benthic habitat mapping [68]–[70], marine mineral exploration [71]–[73] and underwater archaeology [23], [74]. In 2018, Wu *et al.* [75] developed a staring type underwater multispectral imaging (UMSI) system containing 31 narrowband color filters installed on double filter wheels. The detection band range, the number of bands, the spectral resolution, and the detection range of the UMSI system are 400-700 nm, 31, 10 nm, and 0.5-10 m

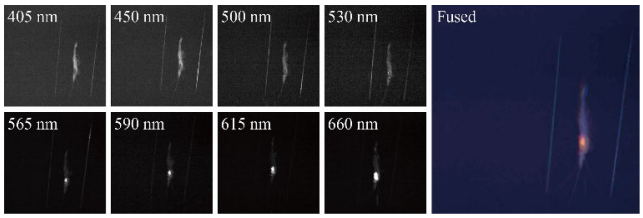

FIGURE 14. Underwater multispectral imaging result by TuLUMIS [76].

respectively. Underwater spectral detection of similar colored targets was conducted in a swimming pool, and the results shown that the UMSI could distinguish spectral features of the similar colored targets, which would contribute to the identification of underwater camouflage targets. In the same year, Liu *et al*. [76] developed a tunable LED-based underwater multispectral imaging system (TuLUMIS), which separated images with different wavebands by switching the light source band. The detection band range, the number of bands, and the spectral resolution of the TuLUMIS are 400-700 nm, 8, 10-100 nm respectively. As presented in Fig. 14, the monochrome images including eight spectral bands are presented on the left, and the fused pseudo-color image is shown on the right. Compared with the traditional underwater imaging system with RGB camera, the TuLUMIS improved the color discrimination by 76.66%. In 2020, Song *et al*. [77] developed a staring type underwater multispectral imaging system based on LCFT, the detection band range, the number of bands, and the spectral resolution of the system are 400-700 nm, 31, and 10 nm respectively. The experimental results in pool and sea shown that the system could obtain the spectral information of underwater static targets in the band of 400-700 nm. Besides, it could also distinguish different objects with similar colors, which is important for identification and classification of the underwater targets.

Underwater spectral imaging has the advantages of high spatial resolution and high spectral resolution, which is suitable for the identification and detection of underwater close objects, mainly applied in the fields of underwater identification of camouflage target, underwater archaeology, and marine mineral exploration. In the future, underwater spectral imaging will develop in the following directions: (i) develop snapshot underwater spectral imaging to increase the spectral imaging rate significantly; (ii) build a more comprehensive spectral database of ocean objects; (iii) reduce the influence caused by suspensions and turbulence; (iv) fusion of image features from the spaceborne, the airborne and the shipborne spectral images to achieve large scale ocean underwater spectral image information acquisition.

F. GHOST IMAGING

Ghost imaging, also known as correlation imaging, was first proposed by Pittman in 1995 [78]. Unlike traditional imaging methods, ghost imaging is based on the correlation properties of the light field, whose imaging quality depends on fluctuations in the detected signal rather than the absolute value of

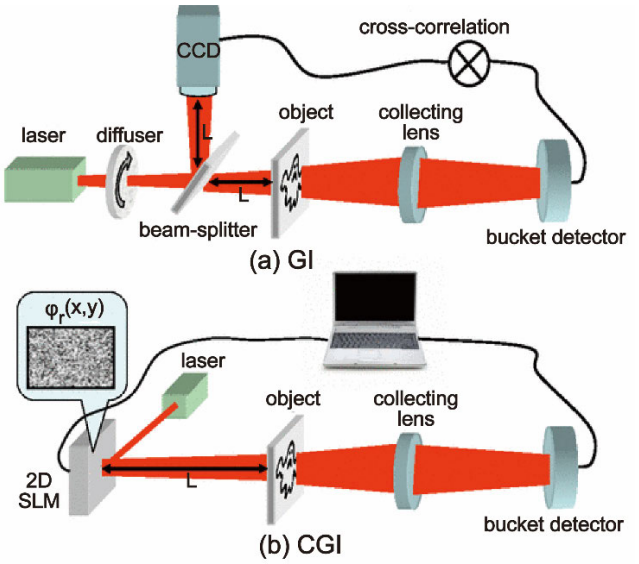

FIGURE 15. Ghost imaging schematic [80].

intensity. It has the advantages of turbulence-free, robustness against scattering [79], and wider angle of view (AOV), which is widely used in biomedical imaging, remote optical sensing, and underwater imaging [24].

Generally, ghost imaging employs pseudothermal light as the light source. According to the different ways of pseudothermal light generation, it can be divided into conventional ghost imaging (GI) and computational ghost imaging (CGI) [80]. The schematic of GI is shown in Fig. 15(a), a pseudothermal beam is generated by a rotating diffuser which is illuminated by a laser. The beam is then divided into two parts by the beam-splitter: one of the beams is the signal beam, which is transmitted (or reflected) by the object and collected by the bucket detector; the other is a reference beam, which is directly received by an area-array detector (such as CCD camera), without passing through any object. By correlating the intensity measured by these two paths, the target image can be reconstructed. Different from GI, CGI generates pseudothermal light by loading a random grayscale map $\varphi_r(x, y)$ on the SLM, as shown in Fig.15(b). Meanwhile, the intensity distribution reflected from the SLM can be calculated according to the scalar diffraction theory, thus the beam splitter and the multi-pixel detector are not required to record the reference light field, and the system is greatly simplified. The system makes use of high-sensitivity single-pixel detector to detect weak signals and improve the underwater detection range. Besides, it improves the imaging resolution by using the spacetime correlation of light intensity fluctuation, reduce the effect of water scattering and turbulence perturbation on imaging quality.

In 2015, Xiang *et al*. [81] introduced a ghost imaging technique into the field of underwater imaging through designing a reflective underwater ghost imaging system, and verified its feasibility in turbid water and long-range underwater imaging. In 2017, Le *et al*. [82] investigated an underwater computational ghost imaging (CGI) at different turbidities

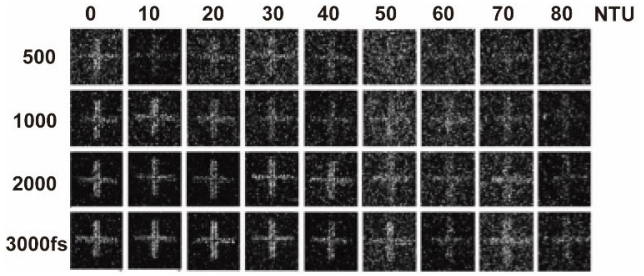

FIGURE 16. Results of CGI. NTU: the unit of turbidity, fs: frames [82].

and angles. The quality of traditional underwater imaging decreases with increasing turbidity, while CGI shows strong robustness for turbidity. As shown in Fig. 16, even in highly turbid water, CGI can still acquire target image as long as sufficient sampling frames are obtained. And the more sampling frames, the higher SNR of the imaging. Moreover, the CGI allows images to be acquired from a wide AOV, which makes it adaptable to harsh underwater environments. In 2019, Zhang *et al*. [83] investigated the influence of ocean turbulence on underwater GI. The results shown that the imaging quality degeneration caused by ocean turbulence was closely related to the propagation distance. The quality of GI can be maintained at a relatively small distance in a strong oceanic turbulence, while the quality degrades sharply at a relatively long distance. Besides, the effect of turbulence on GI caused by temperature fluctuations is more drastic compared to salinity fluctuations.

However, the huge amount of signal acquisitions prevents the development of underwater GI. Compressive sensing (CS), a novel sampling theory, can reduce the cost of storage and transmission. Combination of CS and GI can overcome the limitations of GI mentioned above. In 2019, Chen *et al*. [84] proposed an underwater CGI system based on compressive sensing (CS), which reduced the time spending to acquire data by 70% compared with the traditional CGI. Thus, the combination with CS makes it capable to overcome the limitations of the CGI method such as the long-time data acquisition and the low reconstruction efficiency. Meanwhile, the CS-based underwater CGI system can reconstruct objects even under water with a turbidity up to 80 NTU, which are unavailable for conventional imaging systems.

The characteristics of spectral distribution for the light source have a significant impact on the quality of underwater GI. In 2020, Luo *et al*. [85] first proposed an underwater CGI scheme based on source-shaping technique. By selecting a suitable modulation factor for the shaped Lorentz source, the effects of oceanic turbulence could be effectively mitigated, which improves the imaging distance of CGI.

Underwater ghost imaging fully exploits the transfer and acquisition of underwater information from multiple dimensions such as light field modulation, detection mode, and computational reconstruction, which has the advantages of turbulence-free, weak effect of backscattering, and wider angle of view. Combined with photocounting technique, the maximum detection distance is up to 13.5 AL, which is twice as far as the range-gated imaging. Combined with Compressive Sensing, the visibility of GI can be further enhanced with fewer measurements. In the future, underwater ghost imaging will develop in the following directions: (i) development of more efficient reconstruction algorithms to boost system imaging rates; (ii) investigate ocean channel features to realize imaging in turbulence and scattering mixed environment; (iii) combined with deep learning to further enhance the imaging quality of the system at sub-Nyquist sampling rates.

IV. CONCLUSION AND DISCUSSION

In this review, we firstly summarize underwater optical imaging technologies into two categories: underwater imaging based on image enhancement and underwater imaging based on signal light enhancement. Then, we introduce the theoretical basis of underwater imaging, including the inherent optical properties of seawater, light attenuation properties of seawater, and underwater imaging model. Finally, we highlight the underwater imaging techniques based on signal light enhancement, including range-gated imaging, laser synchronous scanning, polarization imaging, streak tube imaging, spectral imaging, and ghost imaging. In addition, their working principles, technical features, development status and perspective trend are introduced in detail. In summary, we present a comprehensive overview of the principles, advances and challenges of underwater optical imaging, which contributes to the understanding and the development of this field.

Although underwater imaging techniques have made tremendous progress, many issues still need to be addressed. Future works ought to concentrate on the following aspects:

1) Existing underwater imaging techniques cannot solve the conflict between imaging distance and imaging quality. Therefore, it is an important direction for future research to develop an underwater imaging system that can improve the imaging distance and ensure the imaging quality without increasing the complexity of the system.

2) In highly turbid water, the scattering phenomenon caused by particles suspended in the water is aggravated, resulting in the extraction of signal light, thus imaging within highly turbid water is an important direction for future research.

3) Most of the underwater imaging techniques have scene dependence. Therefore, the development of underwater imaging systems with a widely environmental adaptation is one of the future research directions.

4) Alongside with the improvement of hardware configuration, the underwater image enhancement algorithm also needs to be improved. In the future, underwater imaging technology based on signal light enhancement and image enhancement can be combined to achieve high-resolution real-time imaging of underwater long-range targets, which will expand its application scope.

REFERENCES

[1] A. S. A. Ghani and N. A. Mat Isa, "Enhancement of low quality underwater image through integrated global and local contrast correction," *Appl. Soft Comput.*, vol. 37, pp. 332–344, Dec. 2015.
[2] K. Singh, R. Kapoor, and S. K. Sinha, "Enhancement of low exposure images via recursive histogram equalization algorithms," *Optik*, vol. 126, no. 20, pp. 2619–2625, Oct. 2015.
[3] S. Zhang, T. Wang, J. Dong, and H. Yu, "Underwater image enhancement via extended multi-scale retinex," *Neurocomputing*, vol. 245, pp. 1–9, Jul. 2017.
[4] M. A. Mercado, K. Ishii, and J. Ahn, "Deep-sea image enhancement using multi-scale retinex with reverse color loss for autonomous underwater vehicles," in *Proc. OCEANS, Anchorage*, 2017, pp. 1–6.
[5] X. Fu, P. Zhuang, Y. Huang, Y. Liao, X.-P. Zhang, and X. Ding, "A retinex-based enhancing approach for single underwater image," in *Proc. IEEE Int. Conf. Image Process. (ICIP)*, Oct. 2014, pp. 4572–4576.
[6] A. S. A. Ghani and N. A. M. Isa, "Homomorphic filtering with image fusion for enhancement of details and homogeneous contrast of underwater image," *Indian J. Geo-Mar. Sci.*, vol. 44, no. 12, pp. 1904–1919, Dec. 2015.
[7] S. Vasamsetti, N. Mittal, B. C. Neelapu, and H. K. Sardana, "Wavelet based perspective on variational enhancement technique for underwater imagery," *Ocean Eng.*, vol. 141, pp. 88–100, Sep. 2017.
[8] A. Khan, S. S. A. Ali, A. S. Malik, A. Anwer, and F. Meriaudeau, "Underwater image enhancement by wavelet based fusion," in *Proc. IEEE Int. Conf. Underwater Syst. Technol., Theory Appl. (USYS)*, Penang, Malaysia, Dec. 2016, pp. 83–88.
[9] C. O. Ancuti, C. Ancuti, C. De Vleeschouwer, and P. Bekaert, "Color balance and fusion for underwater image enhancement," *IEEE Trans. Image Process.*, vol. 27, no. 1, pp. 379–393, Jan. 2018.
[10] C. Ancuti, C. O. Ancuti, T. Haber, and P. Bekaert, "Enhancing underwater images and videos by fusion," in *Proc. IEEE Conf. Comput. Vis. Pattern Recognit. (CVPR)*, Jun. 2012, pp. 81–88.
[11] K. He, J. Sun, and X. Tang, "Single image haze removal using dark channel prior," *IEEE Trans. Pattern Anal. Mach. Intell.*, vol. 33, no. 12, pp. 2341–2353, Dec. 2011.
[12] C. Li, J. Quo, Y. Pang, S. Chen, and J. Wang, "Single underwater image restoration by blue-green channels dehazing and red channel correction," in *Proc. IEEE Int. Conf. Acoust., Speech Signal Process. (ICASSP)*, Mar. 2016, pp. 1731–1735.
[13] A. Galdran, D. Pardo, A. Picón, and A. Alvarez-Gila, "Automatic red-channel underwater image restoration," *J. Vis. Commun. Image Represent.*, vol. 26, pp. 132–145, Jan. 2015.
[14] J. Y. Chiang and Y.-C. Chen, "Underwater image enhancement by wavelength compensation and dehazing," *IEEE Trans. Image Process.*, vol. 21, no. 4, pp. 1756–1769, Apr. 2012.
[15] P. Drews, Jr., E. D. Nascimento, F. Moraes, S. Botelho, and M. Campos, "Transmission estimation in underwater single images," in *Proc. IEEE Int. Conf. Comput. Vis. Workshops*, Dec. 2013, pp. 825–830.
[16] Y. Wang, J. Zhang, Y. Cao, and Z. Wang, "A deep CNN method for underwater image enhancement," in *Proc. IEEE Int. Conf. Image Process. (ICIP)*, Beijing, China, Sep. 2017, pp. 1382–1386.
[17] C. Fabbri, M. J. Islam, and J. Sattar, "Enhancing underwater imagery using generative adversarial networks," in *Proc. IEEE Int. Conf. Robot. Autom. (ICRA)*, Brisbane, QLD, Australia, May 2018, pp. 7159–7165.
[18] Y.-S. Shin, Y. Cho, G. Pandey, and A. Kim, "Estimation of ambient light and transmission map with common convolutional architecture," in *Proc. OCEANS MTS/IEEE Monterey*, Monterey, CA, USA, Sep. 2016, pp. 1–7.
[19] P. Mariani, I. Quincoces, K. Haugholt, Y. Chardard, A. Visser, C. Yates, G. Piccinno, G. Reali, P. Risholm, and J. Thielemann, "Range-gated imaging system for underwater monitoring in ocean environment," *Sustainability*, vol. 11, no. 1, p. 162, Dec. 2018.
[20] H. Wu, M. Zhao, and W. Xu, "Underwater de-scattering imaging by laser field synchronous scanning," *Opt. Lasers Eng.*, vol. 126, Mar. 2020, Art. no. 105871.
[21] Z. Cui, Z. Tian, Y. Zhang, Z. Bi, G. Yang, and E. Gu, "Research on the underwater target imaging based on the streak tube laser LiDAR," *Proc. SPIE*, vol. 10710, Nov. 2017, Art. no. 107103G.
[22] F. Liu, P. Han, Y. Wei, K. Yang, S. Huang, X. Li, G. Zhang, L. Bai, and X. Shao, "Deeply seeing through highly turbid water by active polarization imaging," *Opt. Lett.*, vol. 43, no. 20, pp. 4903–4906, Oct. 2018.
[23] Ø. Ødegård, A. A. Mogstad, G. Johnsen, A. J. Sørensen, and M. Ludvigsen, "Underwater hyperspectral imaging: A new tool for marine archaeology," *Appl. Opt.*, vol. 57, no. 12, pp. 3214–3223, Apr. 2018.
[24] Y. Zhang, W. Li, H. Wu, Y. Chen, X. Su, Y. Xiao, Z. Wang, and Y. Gu, "High-visibility underwater ghost imaging in low illumination," *Opt. Commun.*, vol. 441, pp. 45–48, Jun. 2019.
[25] R. C. Smith and K. S. Baker, "Optical properties of the clearest natural waters (200–800 nm)," *Appl. Opt.*, vol. 20, no. 2, pp. 177–184, Jan. 1981.
[26] J. S. Jaffe, "Computer modeling and the design of optimal underwater imaging systems," *IEEE J. Ocean. Eng.*, vol. 15, no. 2, pp. 101–111, Apr. 1990.
[27] P. J. Heckman, Jr., "Underwater range gated photography," *Proc. SPIE*, vol. 7, pp. 60–68, Jun. 1966.
[28] J. Busck and H. Heiselberg, "Gated viewing and high-accuracy three-dimensional laser radar," *Appl. Opt.*, vol. 43, no. 24, pp. 4705–4710, Aug. 2004.
[29] W. Xinwei, L. Youfu, and Z. Yan, "Triangular-range-intensity profile spatial-correlation method for 3D super-resolution range-gated imaging," *Appl. Opt.*, vol. 52, no. 30, pp. 7399–7406, Oct. 2013.
[30] M. Laurenzis, F. Christnacher, and D. Monnin, "Long-range three-dimensional active imaging with superresolution depth mapping," *Opt. Lett.*, vol. 32, no. 21, pp. 3146–3148, Nov. 2007.
[31] X. Wang, X. Liu, P. Ren, L. Sun, S. Fan, P. Lei, and Y. Zhou, "Underwater three-dimensional range-gated laser imaging based on triangular-range-intensity profile spatial-correlation method," *Proc. SPIE*, vol. 10020, Oct. 2016, Art. no. 1002006.
[32] F. Christnacher, M. Laurenzis, D. Monnin, G. Schmitt, N. Metzger, S. Schertzer, and T. Scholtz, "3D laser gated viewing from a moving submarine platform," *Proc. SPIE*, vol. 9250, Oct. 2014, Art. no. 920500F.
[33] M. Laurenzis, F. Christnacher, T. Scholz, N. Metzger, S. Schertzer, and E. Bacher, "Underwater laser imaging experiments in the Baltic Sea," in *Proc. SPIE*, vol. 9250, Oct. 2014, Art. no. 920500D.
[34] E. Cametti, S. Dell'Acqua, P. Farinello, G. Piccinno, and G. Reali, "UTOFIA project: A novel MOPA laser source for a compact, cost-effective system for underwater range-gated imaging," in *Proc. 18th Italian Nat. Conf. Photon. Technol.*, Rome, Italy, 2016, pp. 1–4.
[35] P. Risholm, J. Thorstensen, J. T. Thielemann, K. Kaspersen, J. Tschudi, C. Yates, C. Softley, I. Abrosimov, J. Alexander, and K. H. Haugholt, "Real-time super-resolved 3D in turbid water using a fast range-gated CMOS camera," *Appl. Opt.*, vol. 57, no. 14, pp. 3927–3937, May 2018.
[36] X. Liu, X. Wang, P. Ren, Y. Cao, Y. Zhou, and Y. Liu, "Automatic fishing net detection and recognition based on optical gated viewing for underwater obstacle avoidance," *Opt. Eng.*, vol. 56, no. 8, Aug. 2017, Art. no. 083101.
[37] X. Wang, S. Liang, L. Pingshun, F. Songtao, D. Han, Y. Yuqing, Z. Xin, C. Jianan, H. Jun, and Z. Yan, "Underwater 3D triangular range-intensity correlation imaging beyond visibility range (invited)," *Infr. Laser Eng.*, vol. 47, no. 9, Sep. 2018, Art. no. 903001.
[38] M. Wang, X. Wang, L. Sun, Y. Yang, and Y. Zhou, "Underwater 3D deblurring-gated range-intensity correlation imaging," *Opt. Lett.*, vol. 45, no. 6, pp. 1455–1458, May 2020.
[39] M. Rioux, "Laser range finder based on synchronized scanners," *Appl. Opt.*, vol. 23, no. 21, pp. 3837–3844, Nov. 1984.
[40] J. S. Jaffe and C. Dunn, "A model-based comparison of underwater imaging systems," *Proc. SPIE*, vol. 0925, Aug. 1988, pp. 344–350.
[41] S. Ishibashi, Y. Ohta, M. Sugesawa, K. Tanaka, H. Yoshida, and S. K. Choi, "Seabed 3D images created by an underwater laser scanner applied to an AUV," in *Proc. OCEANS, Anchorage*, Anchorage, AK, USA, 2017, pp. 1–5.
[42] Y. Yang, B. Zheng, H.-Y. Zheng, Z.-T. Wang, G.-S. Wu, and J.-C. Wang, "3D reconstruction for underwater laser line scanning," in *Proc. MTS/IEEE OCEANS, Bergen*, Bergen, Norway, Jun. 2013, pp. 1–3.
[43] L. J. Mullen, V. M. Contarino, A. Laux, B. M. Concannon, J. P. Davis, M. P. Strand, and B. W. Coles, "Modulated laser line scanner for enhanced underwater imaging," *Proc. SPIE*, vol. 3761, Oct. 1999, pp. 2–9.
[44] F. R. Dalgleish, F. M. Caimi, W. B. Britton, and C. F. Andren, "Improved LLS imaging performance in scattering-dominant waters," *Proc. SPIE*, vol. 7317, Apr. 2009, Art. no. 73170E.
[45] S. O'Connor, L. J. Mullen, and B. Cochenour, "Underwater modulated pulse laser imaging system," *Opt. Eng.*, vol. 53, no. 5, May 2014, Art. no. 051403.
[46] Z. He, M. Luo, X. Song, D. Wang, and N. He, "Laser line scan underwater imaging by complementary metal–oxide–semiconductor camera," *Opt. Eng.*, vol. 56, no. 12, Dec. 2017, Art. no. 123101.
[47] F. K. Knight, D. I. Klick, D. P. Ryan-Howard, J. R. Theriault, Jr., B. K. Tussey, and A. M. Beckman, "Three-dimensional imaging using a single laser pulse," *Proc. SPIE*, vol. 1103, pp. 174–189, Sep. 1989.

[48] J. Gao, J. Sun, Q. Wang, and M. Cong, "4-D imaging of the short scale ocean waves using a slit streak tube imaging LiDAR," *Optik*, vol. 136, pp. 136–143, May 2017.

[49] C. Ma, S. Han, and P. Wang, "The research on the reconstruction of intensity image based on streak tube imaging LiDAR," *Proc. SPIE*, vol. 7850, Nov. 2010, Art. no. 78500T.

[50] J. Gao, J. Sun, J. Wei, and Q. Wang, "Research of underwater target detection using a slit streak tube imaging LiDAR," in *Proc. Academic Int. Symp. Optoelectron. Microelectron. Technol.*, Harbin, China, Oct. 2011, pp. 240–243.

[51] Z. T. Z. Tian, Z. C. Z. Cui, L. Z. L. Zhang, T. X. T. Xu, Y. Z. Y. Zhang, and S. F. S. Fu, "Control and image processing for streak tube imaging LiDAR based on VB and MATLAB," *Chin. Opt. Lett.*, vol. 12, no. 6, 2014, Art. no. 060015.

[52] J. Gao, J. Sun, and Q. Wang, "Experiments on the range resolution measurement of a slit streak tube imaging LiDAR," *Optik*, vol. 126, no. 21, pp. 3084–3087, Nov. 2015.

[53] M. Chen, Z. He, and F. Ao, "Study and implementation for range-gated underwater laser imaging system," *Proc. SPIE*, vol. 6625, Feb. 2008, Art. no. 66251J.

[54] K. D. Moore, J. S. Jaffe, and B. L. Ochoa, "Development of a new underwater bathymetric laser imaging system: L-bath," *J. Atmos. Ocean. Technol.*, vol. 17, no. 8, pp. 1106–1117, Aug. 2000.

[55] Y. Y. Schechner, S. G. Narasimhan, and S. K. Nayar, "Polarization-based vision through haze," *Appl. Opt.*, vol. 42, no. 3, pp. 511–525, Jan. 2003.

[56] Y. Y. Schechner and N. Karpel, "Clear underwater vision," in *Proc. CVPR*, Washington, DC, USA, 2004, pp. I-536–I-543.

[57] T. Treibitz and Y. Y. Schechner, "Active polarization descattering," *IEEE Trans. Pattern Anal. Mach. Intell.*, vol. 31, no. 3, pp. 385–399, Mar. 2009.

[58] J. Guan, J. Zhu, H. Tian, and X. Hou, "Real-time polarization difference underwater imaging based on Stokes vector," *Acta Phys. Sinica*, vol. 64, no. 22, pp. 141–147, Nov. 2015.

[59] M. Dubreuil, P. Delrot, I. Leonard, A. Alfalou, C. Brosseau, and A. Dogariu, "Exploring underwater target detection by imaging polarimetry and correlation techniques," *Appl. Opt.*, vol. 52, no. 5, pp. 997–1005, Feb. 2013.

[60] Y. Y. Schechner and N. Karpel, "Recovery of underwater visibility and structure by polarization analysis," *IEEE J. Ocean. Eng.*, vol. 30, no. 3, pp. 570–587, Jul. 2005.

[61] B. Huang, T. Liu, H. Hu, J. Han, and M. Yu, "Underwater image recovery considering polarization effects of objects," *Opt. Exp.*, vol. 24, no. 9, pp. 9826–9838, May 2016.

[62] J. D. van der Laan, D. A. Scrymgeour, S. A. Kemme, and E. L. Dereniak, "Increasing detection range and minimizing polarization mixing with circularly polarized light through scattering environments," *Proc. SPIE*, vol. 9099, May 2014, Art. no. 909908.

[63] H. Hu, L. Zhao, X. Li, H. Wang, J. Yang, K. Li, and T. Liu, "Polarimetric image recovery in turbid media employing circularly polarized light," *Opt. Exp.*, vol. 26, no. 19, pp. 25047–25059, Sep. 2018.

[64] H. Hu, L. Zhao, X. Li, H. Wang, and T. Liu, "Underwater image recovery under the nonuniform optical field based on polarimetric imaging," *IEEE Photon. J.*, vol. 10, no. 1, Feb. 2018, Art. no. 6900309.

[65] L. Yang, J. Liang, W. Zhang, H. Ju, L. Ren, and X. Shao, "Underwater polarimetric imaging for visibility enhancement utilizing active unpolarized illumination," *Opt. Commun.*, vol. 438, pp. 96–101, May 2019.

[66] B. Liu, Z. Liu, S. Men, Y. Li, Z. Ding, J. He, and Z. Zhao, "Underwater hyperspectral imaging technology and its applications for detecting and mapping the seafloor: A review," *Sensors*, vol. 20, no. 17, p. 4962, Sep. 2020.

[67] G. Johnsen, Z. Volent, H. Dierssen, R. Pettersen, M. Van Ardelan, F. Søreide, P. Fearns, M. Ludvigsen, and M. Moline, "Underwater hyperspectral imagery to create biogeochemical maps of seafloor properties," in *Subsea Optics and Imaging*. Amsterdam, The Netherlands: Elsevier, 2013, pp. 508–540.

[68] P. A. Letnes, I. M. Hansen, L. M. S. Aas, I. Eide, R. Pettersen, L. Tassara, J. Receveur, S. l. Floch, J. Guyomarch, L. Camus, and J. Bytingsvik, "Underwater hyperspectral classification of deep sea corals exposed to 2-methylnaphthalene," *PLoS ONE*, vol. 14, no. 2, Feb. 2019, Art. no. e0209960.

[69] A. A. Mogstad, G. Johnsen, and M. Ludvigsen, "Shallow-water habitat mapping using underwater hyperspectral imaging from an unmanned surface vehicle: A pilot study," *Remote Sens.*, vol. 11, no. 6, Mar. 2019, Art. no. 685.

[70] F. Foglini, V. Grande, F. Marchese, V. A. Bracchi, M. Prampolini, L. Angeletti, G. Castellan, G. Chimienti, I. M. Hansen, M. Gudmundsen, A. N. Meroni, A. Mercorella, A. Vertino, F. Badalamenti, C. Corselli, I. Erdal, E. Martorelli, A. Savini, and M. Taviani, "Application of hyperspectral imaging to underwater habitat mapping, Southern Adriatic Sea," *Sensors*, vol. 19, no. 10, p. 2261, May 2019.

[71] I. Dumke, S. M. Nornes, A. Purser, Y. Marcon, M. Ludvigsen, S. L. Ellefmo, G. Johnsen, and F. Søreide, "First hyperspectral imaging survey of the deep seafloor: High-resolution mapping of manganese nodules," *Remote Sens. Environ.*, vol. 209, pp. 19–30, May 2018.

[72] O. Sture, M. Ludvigsen, F. Soreide, and L. M. S. Aas, "Autonomous underwater vehicles as a platform for underwater hyperspectral imaging," in *Proc. OCEANS, Aberdeen*, Aberdeen, Scotland, Jun. 2017, pp. 1–8.

[73] Ø. Sture, B. Snook, and M. Ludvigsen, "Obtaining hyperspectral signatures for seafloor massive sulphide exploration," *Minerals*, vol. 9, no. 11, p. 694, Nov. 2019.

[74] Ø. Ødegård, A. J. Sørensen, R. E. Hansen, and M. Ludvigsen, "A new method for underwater archaeological surveying using sensors and unmanned platforms," *IFAC-PapersOnLine*, vol. 49, no. 23, pp. 486–493, 2016.

[75] C. Wu, Y. Shentu, C. Chaofan, Y. Guo, Y. Zhang, H. Wei, P. Yang, H. Huang, and H. Song, "Development of an underwater multispectral imaging system based on narrowband color filters," in *Proc. OCEANS MTS/IEEE Charleston*, Charleston, SC, USA, Oct. 2018, pp. 1–6.

[76] H. Liu, J. Sticklus, K. Koser, H.-J. T. Hoving, H. Song, Y. Chen, J. Greinert, and T. Schoening, "TuLUMIS—A tunable LED-based underwater multispectral imaging system," *Opt. Exp.*, vol. 26, no. 6, pp. 7811–7828, May 2018.

[77] H. Song, Q. Wan, C. Wu, Y. Shentu, W. Wang, P. Yang, W. Jia, H. Li, H. Huang, H. Wang, and S. Zhan, "Development of an underwater spectral imaging system based on LCFT," *Infr. Laser Eng.*, vol. 49, no. 2, Feb. 2020, Art. no. 0203005.

[78] T. B. Pittman, Y. H. Shih, D. V. Strekalov, and A. V. Sergienko, "Optical imaging by means of two-photon quantum entanglement," *Phys. Rev. A, Gen. Phys.*, vol. 52, no. 5, pp. R3429–R3432, Nov. 1995.

[79] Y.-K. Xu, W.-T. Liu, E.-F. Zhang, Q. Li, H.-Y. Dai, and P.-X. Chen, "Is ghost imaging intrinsically more powerful against scattering?" *Opt. Exp.*, vol. 23, no. 26, pp. 32993–33000, Dec. 2015.

[80] Y. Bromberg, O. Katz, and Y. Silberberg, "Ghost imaging with a single detector," *Phys. Rev. A, Gen. Phys.*, vol. 79, no. 5, May 2009, Art. no. 053840.

[81] Q. Xiang, K. Yang, L. Yu, M. Xia, W. Li, and W. Guo, "Reflective underwater ghost imaging," *Acta Opt. Sinica*, vol. 35, Jul. 2015, Art. no. 0711002.

[82] M. Le, G. Wang, H. Zheng, J. Liu, Y. Zhou, and Z. Xu, "Underwater computational ghost imaging," *Opt. Exp.*, vol. 25, no. 19, pp. 22859–22868, Sep. 2017.

[83] Q.-W. Zhang, W.-D. Li, K. Liu, L.-W. Zhou, Z.-M. Wang, and Y.-J. Gu, "Effect of oceanic turbulence on the visibility of underwater ghost imaging," *J. Opt. Soc. Amer. A, Opt. Image Sci.*, vol. 36, no. 3, pp. 397–402, Mar. 2019.

[84] Q. Chen, S. K. Chamoli, P. Yin, X. Wang, and X. Xu, "Active mode single pixel imaging in the highly turbid water environment using compressive sensing," *IEEE Access*, vol. 7, pp. 159390–159401, Nov. 2019.

[85] C.-L. Luo, W.-X. Wan, S.-Y. Chen, A.-F. Long, L.-N. Peng, S.-F. Wu, and H.-R. Qi, "High-quality underwater computational ghost imaging with shaped Lorentz sources," *Laser Phys. Lett.*, vol. 17, no. 10, Oct. 2020, Art. no. 105209.

YING SHEN received the Ph.D. degree from China Agricultural University, China, in 2010. She is currently a Professor with the School of Mechanical Engineering and Automation, Fuzhou University, China. Her research projects include the National Natural Science Foundation of China, the Natural Science Foundation of Fujian Province, the National Defense Science and Technology Key Fund, and the Leading Project of Fujian Science and Technology Department. Her main research interests include computing imaging, optical mechatronic, and optical detection.

CHUANJIANG ZHAO received the B.S. degree from the Henan University of Science and Technology, Luoyang, in 2019. He is currently pursuing the master's degree with the School of Mechanical Engineering and Automation, Fuzhou University, China. His research interests include computing imaging and underwater imaging.

YU LIU received the Ph.D. degree from the Department of Physics, Tsinghua University, in 2019. He joined the College of Mechanical Engineering and Automation, Fuzhou University, as an Associate Professor. His research interests include optoelectronics, micro-photonics, and computing imaging.

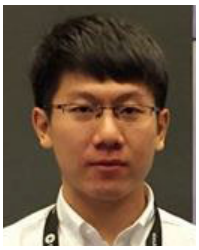

SHU WANG was born in Heilongjiang, China, in 1990. He received the Ph.D. degree in optics from the Key Laboratory of Optoelectronic Science and Technology for Medicine of Ministry of Education, Fujian Normal University, Fuzhou, China. He is currently with the College of Mechanical Engineering and Automation, Fuzhou University, Fuzhou. His main research interests include the computing imaging and the applications of nonlinear optical microscopy in biomedical research.

FENG HUANG was born in Fuzhou, China, in 1979. He is currently with the School of Mechanical Engineering and Automation, Fuzhou University, China. His research interest includes opto-electronic imaging.